Magnetic, electronic and electron transport properties of amorphous $(Co_{0.9}Zr_{0.1})_{100-x}X_x$ (X=Al, Si, Cu, Ge and Zr) pseudo-binary alloys

1992 J. Phys.: Condens. Matter 4 2217

(http://iopscience.iop.org/0953-8984/4/9/015)

J. Phys.: Condens. Matter 4 (1992) 2217–2230. Printed in the UK

Magnetic, electronic and electron transport properties of amorphous $(Co_{0.9}Zr_{0.1})_{100-x}X_x$ (X = Al, Si, Cu, Ge and Zr) pseudo-binary alloys

S Kanemaki†, O Takehira‡, T Goto§ and U Mizutani‡

† Department of Physics, College of General Education, Nagoya University, Furo-cho, Chikusa-ku, Nagoya 464-01, Japan

‡ Department of Crystalline Materials Science, School of Engineering, Furo-cho, Chikusa-ku, Nagoya 464-01, Japan

§ The Institute for Solid State Physics, The University of Tokyo, Roppongi, Minato-ku, Tokyo 196, Japan

Received 2 September 1991, in final form 2 December 1991

Abstract. The magnetic phase diagram is constructed for the amorphous $(Co_{0.9}Zr_{0.1})_{100-x}X_x$ (X = Al, Si, Cu, Ge and Zr) pseudo-binary alloys in the concentration range $0 \leq x \leq 45$ through the DC and AC magnetization measurements in the range 4–800 K. The present results are compared with the previous data for the amorphous Co–Zr binary alloys. The ferromagnetism of the amorphous $Co_{90}Zr_{10}$ master alloy is rapidly weakened and disappears at about $x = 30$, regardless of the third elements Al, Si, Cu and Ge. The concentration dependence of the density of states at the Fermi level is deduced by extracting the band structure contribution from the measured linearly temperature-dependent specific heat coefficient. A significant difference in the electronic structure emerges above $x = 30$, depending on whether the element X added to the $Co_{90}Zr_{10}$ master alloy is a non-transition metal, like Si and Ge, or the transition metal Zr. A rapid increase in the electrical resistivity with increasing x beyond $x = 20$ for the Si and Ge bearing alloys is attributed to a rapidly decreasing density of states at the Fermi level.

1. Introduction

Amorphous Co–Zr alloys are typical of those consisting of early and late transition metals and are characterized by successive appearances of various magnetic states ranging from stable ferromagnetism in the Co-rich end, through the possible spin-glass state and subsequent temperature-dependent paramagnetism in the intermediate range, to a non-magnetic superconducting state in the Zr-rich end (Altounian and Strom-Olsen 1983, Kanemaki *et al* 1989). The photoemission spectroscopy measurements revealed that the valence band of the $Co_{22}Zr_{78}$ amorphous alloy consists of two peaks: the Zr-4d peak near the Fermi level E_F and the Co-3d peak at higher binding energy (Oelhafen *et al* 1980). The band structure calculations for the amorphous $CoZr_3$ alloy confirmed that the above interpretation for the observed UPS spectra is correct (Moruzzi *et al* 1983).

Yamada *et al* (1987a and b) studied the effect of the third elements X = H, B, Al and Si on the electronic structure and the electron transport of the non-magnetic amorphous $Ni_{33}Zr_{67}$ alloy. It was shown that, regardless of the atomic species of the third element

X, the density of states at E_F decreases and the resistivity increases with increasing concentration of X. A reduction in the density of states at E_F was ascribed to the superposition of the two effects: one, the dilution effect of Zr atoms whose 4d-band dominates near E_F and the other the depletion of electrons near E_F to form the bonding states at the binding energies of 7, 4 and 4 eV for the respective third elements H, B and Si embedded in the $Ni_{33}Zr_{67}$ matrix.

In the present work, we studied the magnetic, electronic and the electron transport properties of the amorphous $(Co_{0.9}Zr_{0.1})_{100-x}X_x$ (X = Al, Si, Cu and Ge) pseudo-binary alloys. The temperature dependence of resistivity and the resistivity at 300 K for the amorphous Co–Zr alloys were also measured. The effect of the third elements X = Al, Si, Cu and Ge on the magnetic, electronic and electron transport properties is discussed with reference to the data for the amorphous Co–Zr binary alloys reported earlier by Kanemaki *et al* (1989), which will hereafter be referred to as (I).

2. Experimental procedure

Twenty $(Co_{0.9}Zr_{0.1})_{100-x}X_x$ ternary alloy ingots with X = Si, Al, Cu and Ge in the range $0 \leq x \leq 45$ were prepared by arc-melting appropriate amounts of 99.9%Co, 99.5%Zr, 99.999%Si, 99.999%Al, 99.999%Ge and 99.99%Cu in a high-purity Ar gas atmosphere. The preparation method of the amorphous $Co_{100-x}Zr_x$ binary alloys was reported in (I). Amorphous samples were obtained by using a single-roll spinning wheel apparatus in a reduced Ar gas atmosphere. Exceptions are amorphous Co–Zr alloys containing 20–50 at.%Zr, which were prepared by DC sputtering. The formation of an amorphous phase was confirmed by the x-ray diffraction with Cu–Kα radiation. For the sake of consistency, all samples including the amorphous Co–Zr binary alloys are expressed in the form of $(Co_{0.9}Zr_{0.1})_{100-x}X_x$ and are often abbreviated as X_x. The maximum contents of Si, Al, Cu, Ge and Zr, below which an amorphous single phase was obtained in this experiment, turned out to be x = 45, 15, 5, 35 and 78, respectively.

Low-temperature specific heats were measured in the temperature range 1.5–6 K using an ordinary DC adiabatic method. The DC magnetic susceptibility measurements were carried out in a field up to 6 T in the temperature range 4.2–150 K. The field cooling effect was also examined in a DC field at 20 Oe in the temperature range 4.2–300 K. The AC magnetization was measured in a field amplitude of 10 Oe at 80 Hz in the range 4.2–250 K. The electrical resistivity at 300 K was determined by measuring the average thickness and length of a sample. Its temperature dependence was measured by a DC four-probe method in the range 2–300 K.

3. Results

The saturation magnetization was determined from the field dependence of magnetization up to 6 T at 4.2 K. It turned out that all samples studied are magnetically saturated in a field less than 1 T. The value of the magnetic moment per Co atom is plotted in figure 1 as a function of the content of the third element X. The data in (I) for the amorphous Co–Zr binary alloys are also incorporated by expressing them in the pseudo-binary form $(Co_{0.9}Zr_{0.1})_{100-x}Zr_x$. It may be remarked that the concentration x in the bottom abscissa of figure 1 does not correspond to the total content of Zr in the case of X = Zr, whereas the Co content in the top abscissa does correspond to its net amount

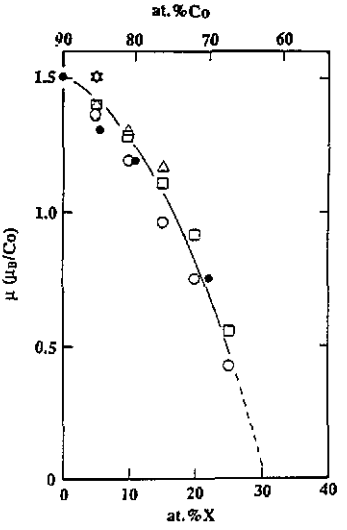

Figure 1. Saturation magnetization per Co atom at 4.2 K as functions of X and Co contents for the amorphous $(Co_{0.9}Zr_{0.1})_{100-x}X_x$ (X = Al, Si, Cu, Ge and Zr) pseudo-binary alloys. The saturation magnetization was determined from the field dependence up to 6 T. Symbols are as follows: (△) X = Al, (○) X = Si, (✡) X = Cu, (□) X = Ge and (●) X = Zr. The data for the X = Zr are reproduced from (I).

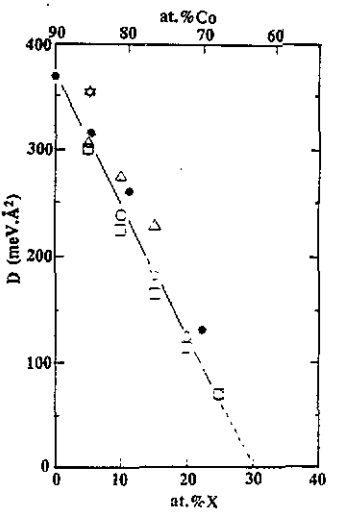

Figure 2. Spin-wave stiffness constant D as functions of X and Co contents for the amorphous $(Co_{0.9}Zr_{0.1})_{100-x}X_x$ (X = Al, Si, Cu, Ge and Zr) pseudo-binary alloys. See symbols in figure 1. The data for the X = Zr are reproduced from (I).

regardless of the atomic species of elements added to the master alloy. It is seen that the value decreases monotonically with decreasing Co content and is extrapolated to zero at about 63 at.%Co or $x = 30$. It is also interesting to note that the extrapolation of the value of the moment shown in figure 1 to greater Co contents gives rise to approximately 1.7 μ_B for the amorphous pure Co, which is in good agreement with the earlier estimate for the amorphous Co–Y alloys by Fukamichi *et al* (1986).

The spin-wave stiffness constant D is deduced by fitting the temperature dependence of magnetization obtained at 1 T to the equations:

$$M(T)/M(0) = 1 - BT^{3/2} - CT^{5/2} \tag{1}$$

and

$$B = [2.61g\mu_B/M(0)](k_B/4\pi D)^{3/2} \tag{2}$$

where μ_B is the Bohr magneton and k_B is the Boltzmann constant. A plot of $M(T)/M(0)$ against $T^{3/2}$ is found to deviate from its linear relation above about 80 K because of the contribution of the final term in (1). Hence, only the low-temperature data were employed for the least-squares fitting without including the final term. As shown in figure 2, the value of D decreases almost linearly with increasing the X content in a manner consistent with the saturation magnetization data. The Curie temperature can be deduced from the temperature dependence of magnetization for Si_x and Ge_x samples with $x = 20$–25. They are listed in table 1, along with other magnetic data. The Curie temperature for the Co-rich ferromagnetic alloys could not be determined because of its location above the crystallization temperature T_x.

Table 1. Magnetic properties of amorphous $(Co_{0.9}Zr_{0.1})_{100-x}X_x$ (X = Al, Si, Cu and Ge) alloys. T_c: Curie temperature. T_f: spin freezing temperature. μ: saturation magnetization at 4 K. D: spin-wave stiffness constant.

	Composition x (at.%Co)	T_c K	T_f K	μ μ_B/Co	D meV Å^2
X = Al	5 (85.5)	*		1.40	307
	10 (81.0)	*		1.30	275
	15 (76.5)	*		1.17	231
X = Si	5 (85.5)	*		1.36	300
	10 (81.0)	*		1.19	238
	15 (76.5)	*		0.96	183
	20 (72.0)	450		0.75	125
	25 (67.5)	170		0.42	70
	30 (63.0)		10		
X = Cu	5 (85.5)	*		1.51	357
X = Ge	5 (85.5)	*		1.40	300
	10 (81.0)	*		1.28	226
	15 (76.5)	*		1.11	165
	20 (72.0)	485		0.92	117
	25 (67.5)	210		0.56	71
	30 (63.0)		20		

† The T_c data indicated by an asterisk cannot be measured because $T_x < T_c$.

The DC magnetic susceptibility and AC magnetization have been measured for magnetically marginal amorphous Si_x and Ge_x alloys in the range $25 \leqslant x \leqslant 45$. The results are shown in figures 3 and 4. The Si_{25} and Ge_{25} samples do not exhibit any cusp in the AC magnetization down to 4.2 K, indicating that they remain ferromagnetic. However, we found hysteresis in the temperature dependence of the DC magnetization for the Si_{25} sample, depending on whether the sample is subjected to field cooling or zero-field cooling. Hence, we believe that the ferromagnetic state is no longer stable in the amorphous Si_{25} alloy and the Ge_{25} as well. The Si_{30} and Ge_{30} alloys show a broad cusp in the AC magnetization curve, indicating that they enter into the spin-glass state at 10–20 K. Figures 3 and 4 also show that all samples with $x \geqslant 35$ are characterized by the temperature-dependent magnetic susceptibility. Combining all magnetic properties obtained, we constructed in figure 5 the magnetic phase diagram for the amorphous $(Co_{0.9}Zr_{0.1})_{100-x}X_x$ alloys.

The low-temperature specific heat data for the Si_x with $x \leqslant 25$, Ge_x with $x \leqslant 25$, Al_x with $x \leqslant 15$ and Cu_x with $x = 5$ can be fitted well to the following equation*

$$C = \gamma T + \alpha T^3 + \sigma_{sw} T^{3/2} + \sigma_n T^{-2} \tag{3}$$

where γ is the electronic specific heat coefficient, α is the lattice specific heat coefficient,

* An additional linearly temperature-dependent specific heat is known to exist in disordered systems including amorphous insulators. This has nothing to do with the electronic specific heat but is associated with the two-level configurational effect inherent in a disordered lattice. Its contribution has been determined to be about 0.06 mJ mol^{-1} K^{-2}, using the specific heat data well below the superconducting transition temperature in the amorphous Cu–Zr alloys (Samwer and Löhneysen 1982). This is two orders of magnitude smaller than the electronic specific heat coefficient discussed in this article. Hence, we ignore this in the rest of the discussion.

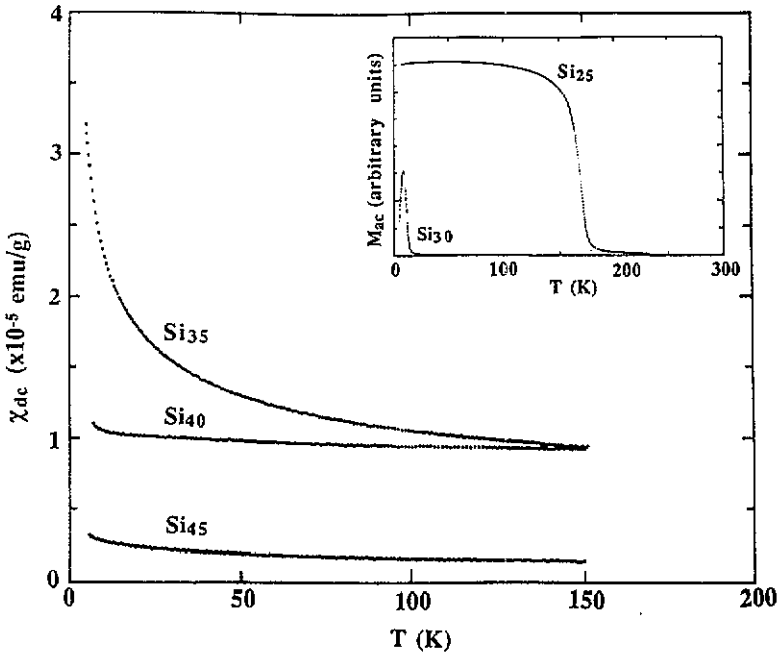

Figure 3. DC magnetic susceptibility as a function of temperature for the amorphous $(Co_{0.9}Zr_{0.1})_{100-x}Si_x$ pseudo-binary alloys. The inset shows the AC magnetization data.

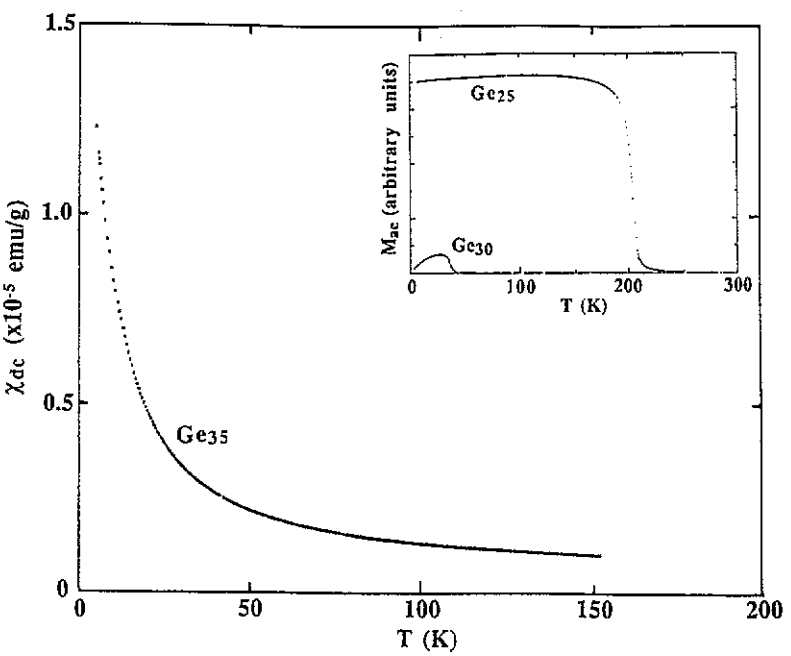

Figure 4. DC magnetic susceptibility as a function of temperature for the amorphous $(Co_{0.9}Zr_{0.1})_{100-x}Ge_x$ pseudo-binary alloys. The inset shows the AC magnetization data.

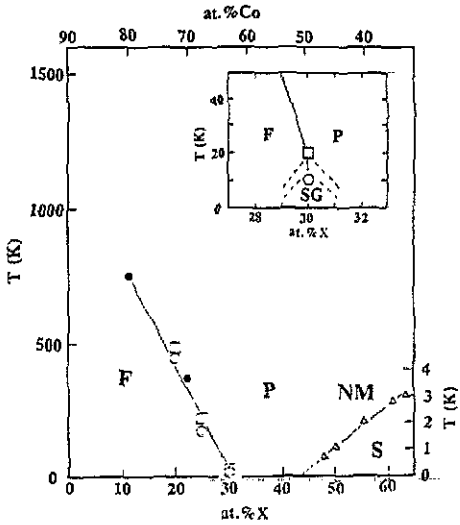

Figure 5. Magnetic phase diagram for the amorphous $(Co_{0.9}Zr_{0.1})_{100-x}X_x$ (X = Al, Si, Cu, Ge and Zr) pseudo-binary alloys. See the symbols in figure 1. The symbol (△) refers to the superconducting transition temperature in the amorphous Co–Zr alloys (Altounian and Strom-Olsen 1983). Symbols F, P, SG, S and NM stand for ferromagnetism, paramagnetism with temperature-dependent magnetic susceptibility, spin-glass, superconducting state and non-magnetic state with temperature-independent magnetic susceptibility, respectively. An inset shows a possible spin-glass region on an expanded scale.

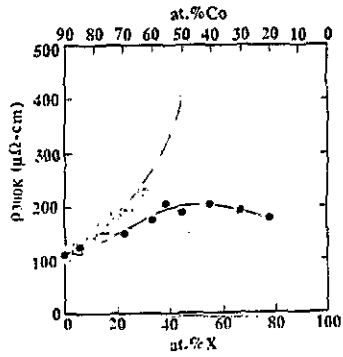

Figure 6. Electrical resistivity at 300 K as functions of X and Co contents in the amorphous $(Co_{0.9}Zr_{0.1})_{100-x}X_x$ (X = Al, Si, Cu, Ge and Zr) pseudo-binary alloys. See the symbols in figure 1.

σ_{sw} is the spin-wave specific heat coefficient and σ_n is the Schottky-type specific heat coefficient associated with the hyperfine splitting of ^{59}Co nuclear energy levels in the internal magnetic field. The four coefficients in (3) cannot be decisively determined by the least squares fitting. Hence, the spin-wave specific heat coefficient σ_{sw} was independently determined from the aforementioned spin-wave stiffness constant D through equation:

$$\sigma_{sw} = 39.431(W/d)D^{-3/2} \tag{4}$$

where W is the atomic weight in g, d is the density in $g\,cm^{-3}$ and σ_{sw} is in mJ mol^{-1} $K^{-5/2}$. The remaining three coefficients γ, α, and σ_n were then determined by the least squares fitting of the specific heat data to (3).

The low-temperature specific heat data for the Si_x alloys with $x \geq 30$ and Ge_x with $x \geq 30$ can be better described in the following equations:

$$C = C_m + \gamma T + \alpha T^3 = A + (\gamma + \gamma_m)T + (\alpha + \alpha_m)T^3 \tag{5}$$

where the magnetic specific heat C_m is approximated as $A + \gamma_m T + \alpha_m T^3$ in its power series expansion in the temperature range 1.5–6 K and, hence, γ_m and α_m possess the same temperature dependences as the electronic and lattice specific heat coefficients, respectively. The coefficient A represents the temperature-independent magnetic specific heat. The validity of (5) in the temperature range of 1.5–6 K has been confirmed

in other magnetically unstable amorphous alloys (Mizutani *et al* 1989a, Kanemaki *et al* 1989). A superposition of the magnetic contribution onto the electronic and lattice specific heat coefficients prevents us from reliably determining the magnitude of the density of states at E_F and the Debye temperature. The low-temperature specific heat data are summarized in table 2.

The electrical resistivity at 300 K is plotted in figure 6 as functions of the X and Co contents. It is found that the resistivity sharply increases with increasing the X content without any indication of saturation for X = Si and Ge. This is in sharp contrast to the data for X = Zr. The temperature dependence of the electrical resistivity is shown in figures 7–9. It can be seen that the resistivity minimum appears in ferromagnetically stable amorphous alloys. The resistivity data below the minimum are fitted to the following equation:

$$\rho(T) = \rho_o - \beta \ln T \tag{6}$$

where β is the logarithmically temperature dependent coefficient. On the other hand, the ρ–T data for non-magnetic amorphous Co–Zr alloys containing more than 50 at.%Zr or with $x \geq 44.4$ consistently exhibit a negative slope with a concave curvature above about 30 K, being typical of the high-resistivity d-electron system (Mizutani 1988a and b). A sharp drop in ρ below a few K is due to the superconducting transition. The resistivity data including the crystallization temperature T_x are listed in table 3.

4. Discussion

4.1. Magnetic properties

The magnetic states observed in the present amorphous $(Co_{0.9}Zr_{0.1})_{100-x}X_x$ pseudo-binary alloys are illustrated in figure 5 in the form of the magnetic phase diagram. It can be seen that the ferromagnetism lasts up to about 30 at.%X (X = Si, Al and Ge) and that the spin-glass state exists at the lowest temperatures in the very limited composition range centred at $x = 30$. Beyond this composition, the temperature-dependent paramagnetism appears and remains up to $x = 45$ for X = Si and Ge.

The data in (I) for the amorphous Co–Zr alloys, which are also incorporated in figure 5, agree well with those for the amorphous alloys with X = Si, Al and Ge in the range $x = 0.30$, indicating that the net Co content is a crucial parameter in determining the magnetic state. The superconductivity is known to appear above 50 at.%Zr in the amorphous Co–Zr alloys (Altounian and Strom-Olsen 1983). Hence, these Zr-rich amorphous alloys are entirely non-magnetic and free from the magnetic enhancement in the low temperature specific heat coefficients.

An insertion of the T^3-coefficient α_{exp} into the expression $\theta_M = [12\pi^4 R/5\alpha_{exp}]^{1/3}$ yields the value of θ_M, where R is the gas constant. Here a suffix 'M' is used instead of a conventional 'D' to emphasize possible incorporation of the magnetic effect through α_{exp}. It reduces to the true Debye temperature θ_D, provided that the magnetic contribution α_m is absent in α_{exp}. The magnetic term α_m, if present, is negative and, hence, results in an unusually small α_{exp} and, in turn, an extremely high θ_M. Figure 10 shows the value of θ_M as functions of the X and Co contents for the present amorphous Co-based alloys. An enhancement in θ_M is found to extend over the composition range $10 < x < 45$ for the alloy systems, particularly, with X = Si and Ge. This suggests that the magnetic specific heat even in ferromagnetic alloys with the Curie temperature above

Table 2. Low-temperature specific heat data for amorphous $(Co_{0.9}Zr_{0.1})_{100-x}X_x$ (X = Al, Si, Cu and Ge) alloys. θ_M is calculated by inserting the value of α_{exp} into the Debye model. The θ_M does not reflect the lattice property when the magnetic contribution is involved in α_{exp}. The value of σ_{sw} in the bracket is calculated by inserting into (4) the measured spin-wave stiffness constant in table 1. The mass density was not measured in the present samples and was therefore estimated using the data for the amorphous Co–Zr alloys measured by Kanemaki *et al* (1989) as a guide.

	Composition x (at.%Co)	γ_{exp} mJ mol^{-1} K^{-2}	α_{exp} $\times 10^{-2}$ mJ mol^{-1} K^{-4}	σ_{sw} mJ mol^{-1} K$^{-5/2}$	σ_n mJ K mol^{-1}	A mJ mol^{-1} K^{-1}	θ_M K	H_{int} KOe
X = Al	5 (85.5)	6.55 ± 0.01	6.13 ± 0.05	(0.0535)	2.70 ± 0.17		317 ± 1	178
	10 (81.0)	6.72 ± 0.01	6.22 ± 0.05	(0.0637)	2.36 ± 0.17		316 ± 1	170
	15 (76.5)	6.98 ± 0.01	3.55 ± 0.04	(0.0833)	1.30 ± 0.14		380 ± 2	130
X = Si	5 (85.5)	6.71 ± 0.02	4.59 ± 0.04	(0.0557)	1.85 ± 0.15		349 ± 1	147
	10 (81.0)	6.91 ± 0.01	3.90 ± 0.03	(0.0793)	1.32 ± 0.16		368 ± 2	128
	15 (76.5)	7.22 ± 0.02	2.83 ± 0.06	(0.119)	1.11 ± 0.20		410 ± 3	120
	20 (72.0)	7.76 ± 0.01	3.31 ± 0.04	(0.213)	0.50 ± 0.12		389 ± 2	83
	25 (67.5)	9.47 ± 0.02	1.97 ± 0.05	(0.512)	0.19 ± 0.15		462 ± 4	54
	30 (63.0)	15.5 ± 0.05	−3.86 ± 0.10			3.21 ± 0.11		
	35 (58.5)	8.31 ± 0.03	0.67 ± 0.07			1.88 ± 0.07	663 ± 22	
	40 (54.0)	4.69 ± 0.03	2.91 ± 0.07			0.47 ± 0.08	406 ± 3	
	45 (49.5)	2.33 ± 0.02	1.03 ± 0.04			0.59 ± 0.05	574 ± 7	
X = Cu	5 (85.5)	6.31 ± 0.02	5.43 ± 0.06	(0.0424)	2.66 ± 0.20		330 ± 1	176
X = Ge	5 (85.5)	6.71 ± 0.01	4.91 ± 0.04	(0.0566)	2.42 ± 0.15		341 ± 1	168
	10 (81.0)	7.03 ± 0.01	6.64 ± 0.05	(0.0890)	2.29 ± 0.19		308 ± 1	168
	15 (76.5)	7.34 ± 0.02	6.46 ± 0.06	(0.147)	2.03 ± 0.20		311 ± 1	163
	20 (72.0)	8.29 ± 0.02	4.03 ± 0.06	(0.254)	0.77 ± 0.22		364 ± 2	103
	25 (67.5)	10.3 ± 0.02	4.29 ± 0.07	(0.546)	0.38 ± 0.19		356 ± 2	74
	30 (63.0)	16.8 ± 0.06	0.94 ± 0.13			2.53 ± 0.15	592 ± 20	
	35 (58.5)	8.78 ± 0.04	5.39 ± 0.09			15.65 ± 0.11	330 ± 2	

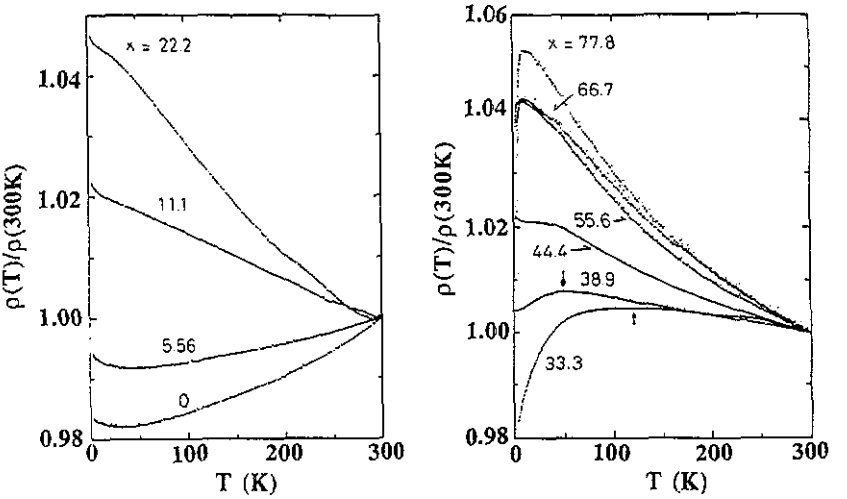

Figure 7. Temperature dependence of the electrical resistivity for the amorphous Co–Zr alloys. The concentration x refers to that in the pseudo-binary form $(Co_{0.9}Zr_{0.1})_{100-x}Zr_x$. The resistivity is normalized with respect to that at 300 K.

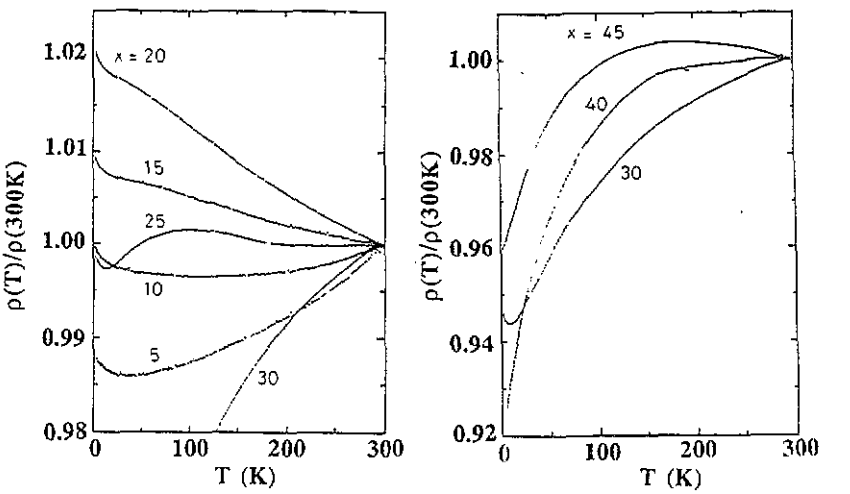

Figure 8. Temperature dependence of the electrical resistivity for the amorphous $(Co_{0.9}Zr_{0.1})_{100-x}Si_x$ pseudo-binary alloys. The resistivity is normalized with respect to that at 300 K.

300 K may not be completely extracted as the spin-wave excitation. Generally speaking, a finite α_m is accompanied by a finite γ_m for magnetically unstable amorphous alloys. Hence, an enhancement in γ_{exp} would be observed in the same composition range as that where an unusually high value of θ_M is observed. It is also noted that the behaviour of θ_M depends rather strongly on the atomic species of the third element in sharp contrast to that of γ_{exp}, which will be discussed in section 4.2.

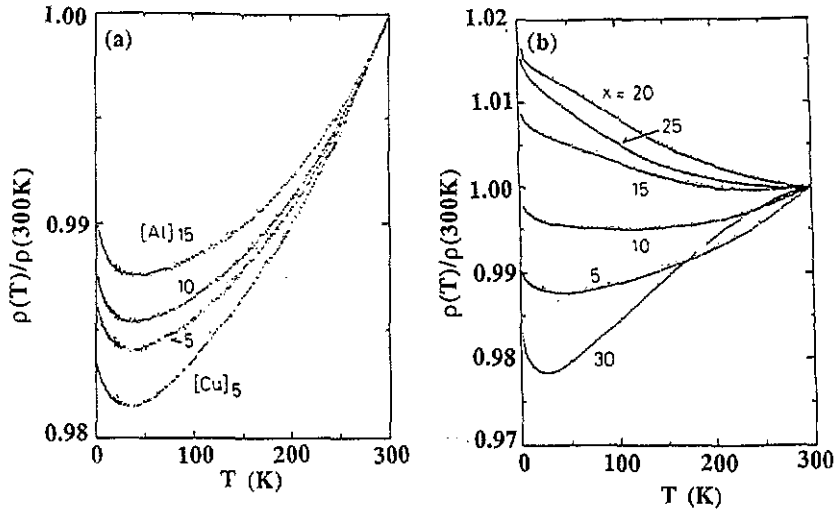

Figure 9. Temperature dependence of the electrical resistivity for the amorphous $(Co_{0.9}Zr_{0.1})_{100-x}X_x$ pseudo-binary alloys with (*a*) X = Al and Cu and (*b*) X = Ge. The resistivity is normalized with respect to that at 300 K.

The internal magnetic field H_{int} can be deduced from the nuclear specific heat coefficient σ_n in (3) by inserting it into the following equation:

$$\sigma_n = xR[(I+1)/3I](4.583\mu_n H_{int}/k_B)^2 \tag{7}$$

where μ_n is the nuclear magneton, I is the nuclear spin of 7/2 for the ^{59}Co nuclei, x is the fraction of Co atoms and R is the gas constant. The resulting value of H_{int} is plotted in figure 11 as a function of the average magnetic moment per Co atom for the various Co-based ferromagnetic amorphous alloys so far studied (Matsuura and Mizutani 1983, Mizutani and Takeuchi 1986, Mizutani *et al* 1987, Kanemaki *et al* 1989). All data, including the present ones, fall on a straight line passing through the origin.

4.2. Electronic structure

The linearly temperature-dependent specific heat coefficient γ_{exp}, which involves the magnetic contribution for the magnetically unstable amorphous alloys, is plotted in figure 12 as a function of the X and Co contents for the amorphous $(Co_{0.9}Zr_{0.1})_{100-x}X_x$ pseudo-binary alloys including those reported in (I). It is interesting to note that, regardless of atomic species of the third elements, the value of γ_{exp} increases sharply with decreasing Co content and forms a huge peak centred at $x = 30$ or 63 at.%Co. This coincides well with the composition where the ferromagnetism collapses and the spin-glass state emerges at the lowest temperatures, as indicated in the magnetic phase diagram in figure 5. The results are also consistent with the data shown in figure 10.

The density of states at E_F has been deduced in (I) from the measured value of γ_{exp} over a whole Zr concentration range for the amorphous Co–Zr alloys. Their treatment is briefly summarized. First, the density of states at E_F for the Zr-rich superconducting phase has been deduced by evaluating the electron–phonon enhancement effect. The enhancement factor λ is obtained by inserting the observed superconducting transition temperature T_c and the Debye temperature θ_D into the McMillan formula (McMillan

Table 3. Electron transport properties of amorphous $(Co_{0.9}Zr_{0.1})_{100-x}X_x$ (X = Zr, Al, Si, Cu and Ge) alloys. T_x: crystallization temperature determined from resistivity measurement with a heating rate of 2 K min^{-1}. ρ_{300K}: resistivity at 300 K. TCR: temperature coefficient of resistivity at 300 K. β: coefficient of (6).

	Composition x (at.%Co)	T_x K	ρ_{300K} $\mu\Omega$ cm	TCR $\times 10^{-5}$ K^{-1}	β $\times 10^{-2}$ $\mu\Omega$ cm ln^{-1} K
X = Zr	0 (90.0)	773	108	10.7	7.3
	5.56 (85.0)	750	128	4.9	13.9
	11.1 (80.0)			−6.0	20.9
	22.2 (70.0)		148	−10.7	19.4
	33.3 (60.0)		175	−5.1	
	38.9 (55.0)	743	208	−3.5	
	44.4 (50.0)	750	187	−5.4	
	55.6 (40.0)	716	209	−8.7	
	66.7 (30.0)		191	−9.8	
	77.8 (20.0)	593	180	−9.9	
X = Al	5 (85.5)	780	123	10.4	9.9
	10 (81.0)	773	124	10.1	10.5
	15 (76.5)		150	9.0	13.7
X = Si	5 (85.5)		135	9.0	12.3
	10 (81.0)	843	136	3.6	13.7
	15 (76.5)	731	170	−1.6	16.4
	20 (72.0)	795	184	−4.9	22.5
	25 (67.5)		198	0.4	16.6
	30 (63.0)		230	6.9	38.1
	35 (58.5)		281	3.2	
	40 (54.0)		350	−5.8	
	45 (49.5)		410		
X = Cu	5 (85.5)	721	116	11.1	9.1
X = Ge	5 (85.5)	733	124	8.4	10.1
	10 (81.0)	684	139	4.8	13.3
	15 (76.5)	683	168	0.5	15.1
	20 (72.0)		181	−1.8	21.4
	25 (67.5)	773	184	−0.2	22.3
	30 (63.0)		222	3.8	54.2

1968). The value of the γ_{band} obtained from $\gamma_{exp}/(1 + \lambda)$ is reproduced in figure 12 as a broken curve 'A' in the range above $x = 45$. On the other hand, the magnetic specific heat for the ferromagnetically stable amorphous $Co_{90}Zr_{10}$ master alloy may well be expressed by the spin–wave term in (3) and, hence, the observed value of γ_{exp} is essentially free from the magnetic contribution. Assuming the electron–phonon enhancement factor λ to be 0.3 for this alloy, Kanemaki *et al* deduced the value of the γ_{band} and connected it smoothly with those values derived for superconducting alloys with $x > 45$.

As shown in figure 12, the value of the γ_{band} monotonically decreases up to about $x = 40$ and then gradually increases in the range $40 < x < 80$ for the amorphous Co–Zr alloys. According to (I), an initial decrease in the γ_{band} with decreasing Co content was interpreted as a decrease in the Co 3d-band height, since the Fermi level is situated there in the Co-rich ferromagnetic regime. However, the Co 3d-band is gradually shifted towards higher binding energies and, instead, the Zr 4d-band grows near the Fermi level

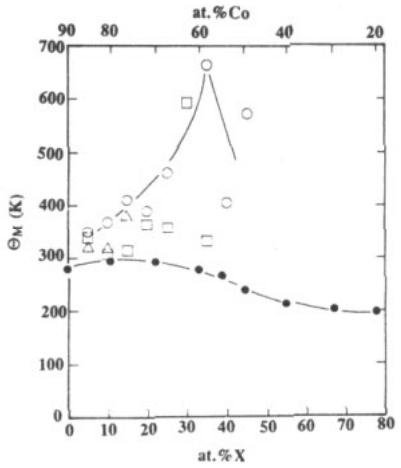

Figure 10. The characteristic temperature θ_M as functions of X and Co contents for the amorphous $(Co_{0.9}Zr_{0.1})_{100-x}X_x$ (X = Al, Si, Cu, Ge and Zr) pseudo-binary alloys. See the symbols in figure 1.

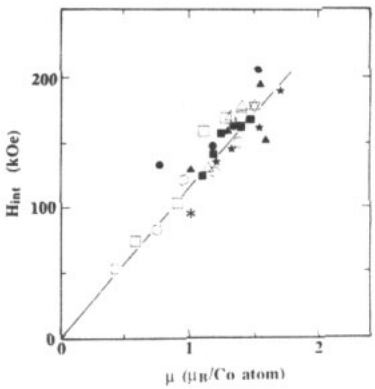

Figure 11. Internal magnetic field H_{int} as a function of saturation magnetization per Co atom in various amorphous Co-based alloys. The same symbols as in figure 1 are used for the amorphous $(Co_{0.9}Zr_{0.1})_{100-x}X_x$ (X = Al, Si, Cu, Ge and Zr) pseudo-binary alloys. Additional symbols refer to the following alloy systems: (■) Co–B (Matsuura and Mizutani 1983); (★) $(Fe_{1-x}Co_x)_{77}B_{13}Si_{10}$; (∗) $(Co_{0.8}Ni_{0.2})_{77}B_{13}Si_{10}$ (Mizutani and Takeuchi 1986); and (▲) Co–Y (Mizutani *et al* 1987). The saturation magnetization for $(Fe_{1-x}Co_x)_{77}B_{13}Si_{10}$ and $(Co_{0.8}Ni_{0.2})_{77}B_{13}Si_{10}$ was calculated per transition metal atom by assuming that all transition metals Fe, Co and Ni equally share the magnetic moment.

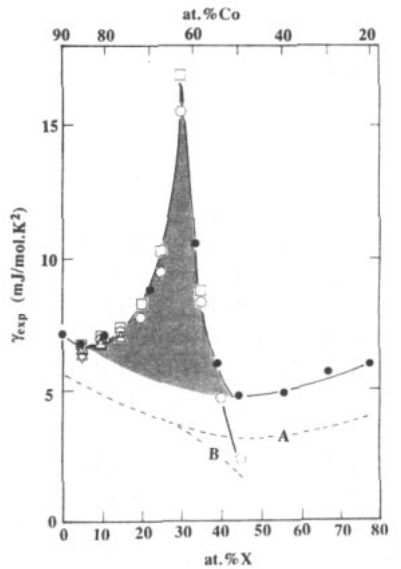

Figure 12. Linearly temperature-dependent specific heat coefficient γ_{exp} as functions of X and Co contents for the amorphous $(Co_{0.9}Zr_{0.1})_{100-x}X_x$ (X = Al, Si, Cu, Ge and Zr) pseudo-binary alloys. The data for the X = Zr are reproduced from (1). Curves 'A' and 'B' represent the band structure contribution for alloys with X = Zr and alloys with X = Si and Ge, respectively. A hatched area represents the magnetic contribution to γ_{exp}. Symbols used are the same as in figure 1.

with increasing Zr content. As a result, the density of states at E_F is dominated by the Zr 4d-states for the Zr-rich superconducting alloys and, thus, the γ_{band} begins to increase with increasing Zr content. This explains the reversal of the slope in the γ_{band} at about $x = 40$.

The situation should differ when the third element is chosen from the non-transition metal elements like Si and Ge. Indeed, the value of γ_{exp} for Si_{45} is fairly small, indicating essentially the absence of a magnetic contribution. A broken curve 'B' is drawn in figure 12 by assuming the electron–phonon enhancement factor to be 0.3. It is seen that the density of states at E_F for these metalloid-bearing alloys decreases continuously beyond $x = 40$, because these electrons do not carry the d-electrons as opposed to Zr. This analysis may be justified from the similar results obtained for the amorphous $(Ni_{33}Zr_{67})_{1-x}X_x$ (X = H, B, Al and Si) ternary alloys (Yamada *et al* 1987a). The magnetic contribution to γ_{exp} is now obvious and its area, bounded by the measured γ_{exp} and $(1 + \lambda)\gamma_{band}$ values, is shown by hatches in figure 12.

4.3. Electron transport properties

Mizutani *et al* (1990a and b) and Mizutani (1991) have discussed the interrelationship between the resistivity and the density of states at E_F for non-magnetic amorphous and quasicrystalline alloys in terms of the Drude expression for the resistivity:

$$\sigma = ne^2\tau/m = (e^2/3)N(E_F)\Lambda_F v_F \tag{8}$$

where $N(E_F)$ is the density of states at E_F, v_F is the Fermi velocity and Λ_F is the mean free path of conduction electrons. In the high resistivity limit, it was claimed that the mean free path Λ_F is constrained by an average atomic distance of about 4 Å and v_F is reduced by the factor g of about 0.2 relative to the free electron value of 10^8 cm s^{-1}. This condition is applied to both non-magnetic sp- and d-electron systems and the high-resistivity limiting curve is drawn in the resistivity versus electronic specific heat coefficient map. The data appearing immediately below this curve are always characterized by the unique temperature dependence of resistivity with a negative TCR over a whole temperature range (they are referred to as types (d) or (e)). As shown in figure 7, the ρ–T data for non-magnetic amorphous Co–Zr alloys containing more than 50 at.%Zr or $x \geq 44.4$ in the pseudo-binary expression are indeed well characterized by the type (e).

In the preceding section, we pointed out that there exists a distinctive difference in the behaviour of the resistivity at 300 K between the alloys with X = Si, Al and Ge and those with X = Zr. As can be understood from the above argument, a large resistivity observed in the Si_x and Ge_x with $x > 30$ may well be attributed to a substantial decrease in the density of states at E_F relative to that for the Co–Zr alloys. Judging from the magnitudes of the resistivity and the electronic specific heat coefficient, we expect the ρ–T types of (d) or (e) to occur in such high-resistivity amorphous alloys. However, as shown in figures 8 and 9, the slope of the resistivity or TCR in amorphous Si_x and Ge_x alloys with $x > 30$ is mostly positive and does not obey the general rule on the ρ–T types established for non-magnetic amorphous alloys (Mizutani *et al* 1990a). Although the distinctive difference in the magnitude of resistivity between the Si_x and Ge_x alloys and the Zr_x alloys can be explained by the difference in the carrier density at E_F, we have to admit that the complicated magnetic effect, as reflected by the temperature-dependent magnetic susceptibility, makes the analysis of its temperature dependence more difficult and delicate. For example, the ρ–T dependence for the ferromagnetic Si_x alloys with

$x = 15$–20 in figure 8 looks similar to the ρ–T curve of type (e) observed for high-resistivity non-magnetic amorphous alloys. Further work is needed to check if the analysis based on the temperature derivative of conductivity, which has been proved to be successful in extracting the magnetic effects in the amorphous Ni–Zr–X (X = Mn, Fe, etc) alloys, can be applied to the present system (Mizutani *et al* 1989b).

References

Altounian Z and Strom-Olsen J O 1983 *Phys. Rev.* B **27** 4149

Fukamichi K, Goto T, Satoh Y, Sakakibara T, Todo S, Mizutani U and Hoshino Y 1986 *IEEE Trans. Magn.* **MAG-22** 555

Kanemaki S, Takehira O, Fukamichi K and Mizutani U 1989 *J. Phys.: Condens. Matter* **1** 5903

Matsuura M and Mizutani U 1983 *J. Phys. F: Met. Phys.* **13** 1539

McMillan W L 1968 *Phys. Rev.* **167** 331

Mizutani U 1988a *Mater. Sci. Eng.* **99** 165

—— 1988b *Suppl. Trans. JIM* **29** 275

—— 1991 *Materials Science and Technology A Comprehensive Treatment* vol 3 ed R W Cahn, P Haasen and E J Kramer (Weinheim, Federal Republic of Germany: VCH) Ch 9 at press

Mizutani U, Fukamichi K and Goto T 1987 *J. Phys. F: Met. Phys.* **17** 257

Mizutani U, Hasegawa M, Fukamichi K, Goto T and Matsuda T 1989a *Mat. Trans. JIM* **30** 953

Mizutani U, Mishima C and Goto T 1989b *J. Phys.: Condens. Matter* **1** 1831

Mizutani U, Ohashi S, Matsuda T, Fukamichi K and Tanaka K 1990a *J. Phys.: Condens. Matter* **2** 541

Mizutani U, Sakabe Y, Shibuya T, Kishi K, Kimura K and Takeuchi S 1990b *J. Phys.: Condens. Matter* **2** 6169

Mizutani U and Takeuchi M 1986 *J. Phys. F: Met. Phys.* **16** 79

Moruzzi V L, Oelhafen P, Williams A R, Lapka R, Güntherodt H-J and Kübler J 1983 *Phys. Rev.* B **27** 2049

Oelhafen P, Hauser E and Güntherodt H-J 1980 *Solid State Commun.* **35** 1017

Samwer K and von Löhneysen H 1982 *Phys. Rev.* B **26** 107

Yamada Y, Itoh Y, Mizutani U, Shibagaki N and Tanaka K 1987a *J. Phys. F: Met. Phys.* **17** 2303

Yamada Y, Itoh Y, Matsuda T and Mizutani U 1987b *J. Phys. F: Met. Phys.* **17** 2313